Extended X-ray Absorption Fine Structure Studies on the Structure of the Poly(vinylpyrrolidone)-Stabilized Cu/Pd Nanoclusters Colloidally Dispersed in Solution

Cui-Rong Bian, Shushi Suzuki, and Kiyotaka Asakura*

Catalysis Research Center, Hokkaido University, Kita-ku, Sapporo 060-0811, Japan

Lu Ping and Naoki Toshima

Department of Materials Science and Engineering, Science University of Tokyo in Yamaguchi, Onoda-shi, Yamaguchi 756-0884, Japan

Received: February 21, 2002; In Final Form: April 25, 2002

Polymer-protected Cu/Pd bimetallic nanoclusters colloidally dispersed in a glycol solution were investigated by means of extended X-ray absorption fine structure (EXAFS). Cu/Pd alloy structures were observed in a wide range of Cu/Pd composition. Shorter Cu−Pd bond distances and more coordination numbers of Cu around Pd and Pd around Cu were found for the nanoclusters with Cu/Pd = 4:1, 3:2, and 1:1 than those expected in random alloy structures, indicating stronger interaction between Cu and Pd atoms. We proposed a "heterobond-philic" model for a new type of bimetallic nanoclusters. The preferential formation of the Cu−Pd bond may be the origin for the unique catalytic properties for hydration and hydrogenation reactions.

1. Introduction

Nanoclusters draw much attention in physics and chemistry because they show quite different properties from their bulk counterparts because of the so-called "quantum size effect".[1] The nanoclusters are also important in industrial fields such as catalysts, sensors, electronic devices, magnetic materials, and optics.[2] Stable nanoclusters with monometallic and bimetallic composition colloidally dispersed in solutions were prepared in the presence of the protecting polymers.[3−5] They are characterized by many techniques, such as UV−vis, X-ray diffraction analysis (XRD), transmission electron microscopy (TEM), x-ray photoelectron spectroscopy (XPS), small-angle X-ray scattering, and energy-dispersed microanalysis.[6] N. Toshima and co-workers prepared poly(vinylpyrrolidone) (PVP)-stabilized Cu/Pd clusters by the reduction of PVP-protected Cu/Pd bimetallic hydroxide by glycol. The Cu/Pd bimetallic clusters showed selective hydrogenation of 1,3-cyclooctadiene and hydration of acrylonitrile.[7,8] This method gave bimetallic nanoclusters in a wider range of Cu/Pd ratio than the thermal decomposition methods.[9,10] The characterization of the colloidal Cu/Pd nanoclusters prepared from the hydroxide nanoparticles has been performed by TEM, UV−vis, XPS, Raman, XRD, and X-ray absorption fine structure (XAFS), which indicated the presence of a random alloy structure.[11,17] However, the atomic level structures inside the Cu/Pd nanoclusters were unclear yet. In this paper, we investigated the detailed structure of the colloidally dispersed Cu/Pd nanoparticles by means of extended X-ray absorption fine structure (EXAFS).

EXAFS is referred to an oscillation appearing in an X-ray absorption spectrum, 50−1000 eV above the absorption edge, involving the information about the local structure around the X-ray absorbing atoms such as bond distances and coordination numbers.[12] In bimetallic particles, EXAFS spectroscopy has another advantage.[13] EXAFS oscillations could be analyzed from both absorption edges of the component elements in bimetallic particles. Previously, Toshima and co-workers had applied EXAFS to bimetallic nanoparticles colloidally dispersed in solutions, such as Pd/Au, Pd/Pt, Rh/Pt, and so on.[6,14−16] Comparing the coordination numbers around each absorbing atom with those calculated from the corresponding model structure, one could elucidate the distribution of the atoms inside the particles. Toshima and Yonezawa have proposed three types of inner structure.[6] One is a core−shell structure in which one metal component is preferentially situated inside the particle and the other is located in the surface region. PVP-stabilized Pt/Pd and Au/Pd (1/4) bimetallic clusters are reported to possess this core−shell structure. The second is a random alloy structure in which each component is mixed with each other. This structure is proposed for Cu/Pd nanoparticles.[17] The third type is a cluster-in-cluster structure in which like atoms get together to form small clusters and the small clusters randomly mixed up to form a larger cluster (or supercluster following the Schmid's definition).[3] Pt/Pd supported on SiO_2 and Pd/Au (1/1) bimetallic particles have this "cluster-in-cluster" structure.[15,18] In this case, homobond pair is preferentially formed, and thus, we can call the cluster-in-cluster as a "homobond-philic" structure. In this paper, we proposed the fourth type of structure model for bimetallic clusters, the so-called "hetero-bond-philic structure" in which the Pd−Cu bond is preferentially formed.

2. Experimental Section

2.1. Sample Preparation. Colloidal dispersions of Cu/Pd were prepared as described in detail elsewhere.[7,8] The $Pd(OAc)_2$ (OAc = acetate) in dioxane solution was added to PVP (PVP = poly(*N*-vinyl-2-pyrrolidone)) and $Cu(SO_4)$ glycol solution at 0−5 °C, followed by the adjustment of the solution pH to 10 using a NaOH aqueous solution. Polymer-stabilized colloidal metal hydroxide thus obtained was then reduced by refluxing the solution at 198 °C for 3 h with a nitrogen flow passing through the reaction system.

* To whom correspondence should be addressed. Tel and Fax: 81-11-706-3671. E-mail: askr@cat.hokudai.ac.jp.

10.1021/jp0204861 CCC: $22.00
Published on Web 08/02/2002

2.2. EXAFS Measurements. EXAFS measurements were carried out in Photon Factory, Institute for Material Structure Science (KEK-IMSS-PF, Proposal No. 95G003). The energy and current of the storage ring were 2.5 GeV and 300 mA, respectively. Cu K-edge (8.9 keV) EXAFS spectra were recorded at a BL12C beam line where a Si(111) double crystal monochromator was installed.[19] The monochromatized beam was focused using a Rh-covered bent cylindrical mirror with a cutoff energy at 23 keV. N_2 and 25% Ar-mixed N_2 gases were filled in I_0 and I ionization chambers to detect X-rays, respectively. Higher harmonics (third-order or higher) were rejected by detuning the monochromator, a bent mirror, adjustment of the sample thickness ($\mu t < 3$), and the choice of appropriate detection gases. Pd K-edge (23 keV) EXAFS measurements were carried out at a BL10B beam line using a Si(311) channel cut monochromator.[20] Ar and Kr were filled in I_0 and I ionization chambers, respectively. Because the ring energy of PF is 2.5 GeV, the third-order higher harmonics (~70 keV) is negligibly small in the Pd K-edge energy region. At the same time, the sample thickness was adjusted to give the total absorbance less than 3. The samples were transferred to glass-made sample cells with Kapton windows under the N_2 atmosphere. Typical sample thicknesses were 0.5 and 2 cm for Cu and Pd edges, respectively.

2.3. Analysis of EXAFS. EXAFS analyses were carried out using an analysis package, "REX" or "REX2001", coded by Rigaku company. We briefly describe the analysis procedure.[21] The EXAFS oscillations, $\chi(k)$, were elucidated from the data by a spline smoothing method and normalized by the edge height, the energy dependence of which was determined from McMaster parameters. The k^3-weighted EXAFS data over 30−150 nm^{-1} were Fourier-transformed into r space and the main peak region (typically 0.12−0.28 nm) was filtered and inversely Fourier-transformed into k space. By adopting k^3-weight, the effect of the coordination of PVP can be minimized because the EXAFS oscillations for N and O appear at low k regions. The data were then analyzed by the curve fitting methods in k space using a following equation.

$$\chi(k) = \sum_i \frac{S_i N_i F_i(k_i)\, e^{-2\sigma_i^2 k_i^2}}{k_i r_i^2} \sin(2k_i r_i + \varphi_i(k_i))$$

$$k_i = \sqrt{k^2 - 2m_e \Delta E_i/\hbar^2} \qquad (1)$$

where S_i, N_i, σ_i, and r_i, are an inelastic reduction factor, a coordination number, a Debye−Wallor factor, and a bond distance for i-th shell. $F_i(k)$ and $\phi_i(k)$ are a backscattering amplitude and a phase shift function for i-th shell, respectively. The phase shift and amplitudes were calculated using FEFF8.[22] Their validity was checked by alloy foils. ΔE_i is a difference between experimentally determined photoelectron kinetic energy zero and that used for theoretical calculation for phase shift and amplitude functions of the i-th shell. S_i was estimated by the comparison with the foil data. Degree of fitting was evaluated with R factor defined as follows.

$$R = \frac{\sum (k^3\chi_{obs}(k) - k^3\chi_{calc}(k))^2}{\sum (k^3\chi_{obs}(k))^2} \qquad (2)$$

The S/N ratios were calculated as follows.

$$S/N = \frac{\sum \{\chi_{obs}(k)\}^2}{\sum \epsilon^2} \qquad (3)$$

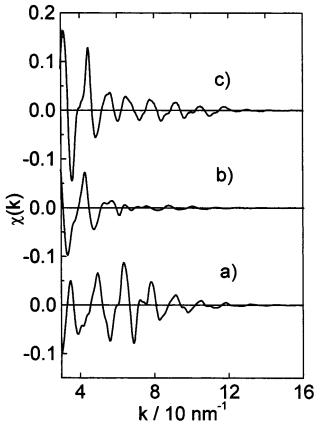

Figure 1. Cu K-edge EXAFS oscillations of (a) Cu and Cu/Pd foils with Cu/Pd atomic ratio = (b) l:l and (c) 1:9.

where ϵ is a statistic error estimated from the Fourier transformation of 150−250 nm^{-1} according to the literature.[23]

In a bimetallic system, EXAFS data are often analyzed using the double edge simultaneous fitting routine in which the fitting is carried out with rigorously satisfying the following conditions.[13]

$$N_{PdCu} C_{Pd} = N_{CuPd} C_{Cu}$$

$$r_{CuPd} = r_{PdCu} \qquad (4)$$

where N_{PdCu}, N_{CuPd}, C_{Pd}, and C_{Cu} are the coordination number of Cu in the first shell of Pd, the coordination number of Pd in the first shell of Cu, and atomic fractions of Pd and Cu, respectively. This relationship is always physically valid independent of the structural details of the system. However, at the present stage of theory, these equations are only fulfilled allowing a certain amount of errors in coordination numbers and bond distances. Therefore, the rigorous application of the eq 4 may shove off the error to the rest of structural parameters. We carried out the curve fittings for the Cu K-edge and the Pd K-edge EXAFS oscillations separately and checked that the relationships (eq 4) are satisfied within the limit of errors. In the nanocluster, a radial distribution function is often reported to be asymmetric so that one may adopt a cumulant expansion method to assess the asymmetric radial distribution.[24−27] However, we could not adopt this method because we needed at least two more fitting parameters for each shell, which would create large correlations among fitting parameters and would diminish the accuracy and precision of the fitting results. We discuss the effect of asymmetrical radial distribution later.

3. Results

3.1. EXAFS. *3.1.1. EXAFS Results on Pd, Cu, and Cu/Pd Alloy Foils.* To see the validity of phase shift and amplitude functions derived from FEFF, as well as to determine S_0, we carried out analyses of Cu, Pd, and Cu/Pd alloy foils. Figures 1 and 2 show the Cu K-edge and Pd K-edge EXAFS oscillations of Cu, Pd, and Cu/Pd alloy foils, respectively. The EXAFS oscillation for Cu foil has a maximum around 70 nm^{-1}. For Pd foil, the strong EXAFS oscillation appears around 30 nm^{-1} and it lasts up to about 160 nm^{-1}. This is due to the different k-dependence of scattering amplitudes for Cu and Pd scatterers.[28] In the Cu/Pd alloy foil with the ratio of Cu/Pd = 1:9, the maximum in the Cu K-edge EXAFS oscillation appears at 30 nm^{-1} and the oscillation lasts up to high k region similar to Pd foil, indicating that Cu is dominantly surrounded by Pd atoms.

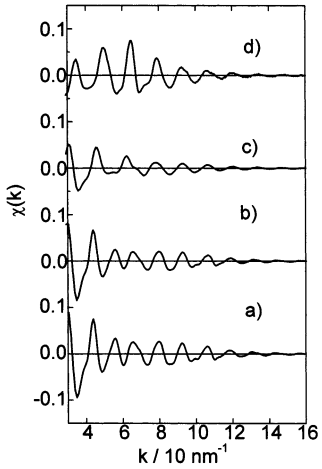

Figure 2. Pd K-edge EXAFS oscillations of (a) Pd and Cu/Pd foils with Cu/Pd atomic ratio = (b) 1:9, (c) 1:1, and (d) 9:1.

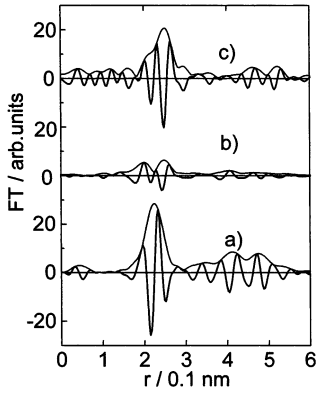

Figure 3. Imaginary and absolute parts of Fourier transforms for k^3-weighted Cu K-edge EXAFS oscillations of (a) Cu foil and Cu/Pd alloy foils with Cu/Pd atomic ratio = (b) l:1 and (c) 1:9.

Conversely, Pd K-edge EXAFS oscillation of the Cu/Pd alloy foil with the ratio of Cu/Pd = 9:1 gave its maximum at 70 nm^{-1} at the same position as found in Cu foil, suggesting Pd is mainly surrounded by Cu atoms. One should note that the Cu and Pd K-edge EXAFS oscillatons for Cu/Pd alloy foil with 1:1 are small in their amplitudes as shown in Figures lb and 2c. This is a so-called interference effect of the oscillations with slightly different wavelengths arising from Cu−Cu and Cu−Pd bonds (or Pd−Pd and Pd−Cu bonds), which diminish the amplitude of the oscillations.

Figure 3 shows the Cu K-edge k^3-weighted Fourier transforms of EXAFS over 30−150 nm^{-1}. As reported in a previous paper,[17] the Fourier transform peak of the Cu K-edge EXAFS in Cu/Pd alloy decreased in its amplitude and was split into two peaks with the increase of the Pd content. When the Pd content exceeded 1:1, the main peak grew in its intensity and shifted to a longer position. This change can be understood on the basis of the interference effect as mentioned above. Thus the split peak cannot be directly assigned to a specific bond like Cu−Cu or Cu−Pd.[21]

Figure 4 shows the Fourier transforms of Pd K-edge EXAFS. The main peak was first reduced and then increased with the increase of Cu content and shifted to a lower bond-length side.

The curve-fitting results are summarized in Table 1, together with the crystallographic data. In the previous work on Pt/Pd, we used empirical phase and amplitude functions derived from Pt/Pd 1:9 and 9:1 alloy foils.[18] In that case, we postulated the bond length of Pt−Pd to be equal to the average value of Pt−Pt and Pd−Pd bond distances because the bond lengths of

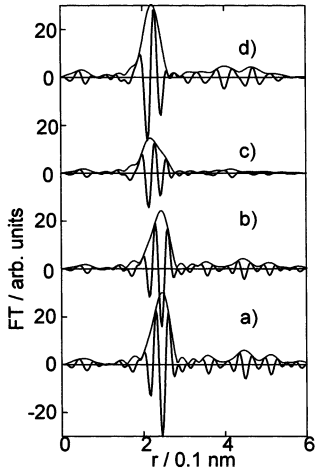

Figure 4. Imaginary and absolute parts of Fourier transforms for k^3-weighted Pd K-edge EXAFS oscillations of (a) Pd foil and Cu/Pd alloy foils with Cu/Pd atomic ratio = (b) 1:9, (c) 1:1, and (d) 9:1.

Pt−Pt (0.278 nm) and Pd−Pd (0.274 nm) were not so different from each other, which would not give a serious error in the final fitting results. On the other hand, in the Cu/Pd case, it is dangerous to postulate that Cu−Pd and Pd−Cu bond distances should be equal to the average value of Cu−Cu and Pd−Pd because Cu−Cu distance in Cu foil is 0.02 nm shorter than Pd−Pd distance. Thus, we adopted theoretical standards calculated from FEFF8. Phase shift and amplitude functions given by FEFF are dependent on the bond length and chemical environment. FEFF8 calculations were carried out in the following three extreme cases: (1) Cu is surrounded by *12 unlike atoms* (Pd atoms) and all atoms are located at Cu lattice points (*Cu−Pd bond length = 0.255 nm*). (2) Cu is surrounded by *1 unlike atom together with 11 like atoms* (*Cu−Pd bond length = 0.255 nm*). (3) Cu is surrounded by *12 unlike atoms* and all atoms are at Pd lattice points (*Cu−Pd bond length = 0.274 nm*).

In three cases, we assumed an fcc structure. A little difference was found at less than 60 nm^{-1} in their amplitude and phase shift functions for Cu−Pd as shown in Figure 5. The errors in phase shift and amplitude functions will transfer to the errors in distances and coordination numbers, respectively. We evaluated the errors in the distances and coordination numbers arising from these small differences in phase shift and amplitude functions by fitting the EXAFS of the case 3 with the phase and amplitude functions derived from model structures of case 1 and case 2. In both cases, the distances and coordination numbers are determined as 0.274 nm and 11.9 for case 1 as a model and 0.274 nm and 12.1 for case 2 as a model, respectively. The similar difference was found in the Pd−Cu bond calculations for Pd K-edge using different structures. Thus, the errors arising from the selection of model structures for the calculations of phase shift and amplitude could be negligible for bond distance and less than 2% for coordination number.

Figures 6 and 7 show the curve fitting results of EXAFS data using parameters derived from FEFF8 for Cu and Pd foils, respectively. The FEFF8-derived phase shift and amplitude functions reproduce very well the EXAFS oscillation for the first shell of Cu foil. The structural parameters derived from the best-fit results are shown in Table 1. As reported before, excellent fitting results can be obtained with 0.002−0.003 nm shorter Cu−Cu distance than the crystallographical data (0.2556 nm).[29] This may be the systematic error arising from the EXAFS analyses. Because of the denominator of the $1/r^2$ term in eq 1, the bond distance derived from EXAFS is shifted from the top value of the radial distribution function by $2\sigma^2/r$. Moreover, if

TABLE 1: Curve-Fitting Results of Cu, Pd, and Cu/Pd Alloy Foils

sample	edge	bond	N	r, nm	ΔE, eV	$\Delta\sigma^2$, 10^{-5} nm^2	R, %	S/N
Cu foil	Cu	Cu−Cu	[12][b]	0.253 (0.002) [0.256][b]	3.5	4.6	0.1	250
Pd foil	Pd	Pd−Pd	[12][b]	0.274 (0.002) [0.276][b]	−4.0	1.1	3.1	142
Pd foil[a]	Pd	Pd−Pd	[12][b]	0.274 (0.002) [0.276][b]	−3.0	1.1	0.5	
Cu/Pd 1:9 foil	Cu	Cu−Cu	[1.2][b]	0.259 (0.006)	−1 (8)	4.5 (1.5)	1.6	89
		Cu−Pd	[10.8][b]	0.268 (0.002)	−5 (3)	3.0 (1.0)		
	Pd	Pd−Cu	1.3 (0.4)	0.267 (0.004)	−5.4 (5)	2.0 (1.5)	0.9	170
		Pd−Pd	10.6 (0.5)	0.272 (0.002)	−1.2 (3)	2.0 (1.0)		
Cu/Pd 1:1 foil	Cu	Cu−Cu	6.2 (0.5)	0.257 (0.003)	−4 (4)	5.0 (1.5)	1.9	105
		Cu-Pd	5.9 (0.5)	0.262 (0.004)	7 (4)	4.5 (1.5)		
	Pd	Pd−Cu	6.1 (0.5)	0.262 (0.003)	−4 (5)	4.0 (1.5)	2.4	85
		Pd−Pd	5.8 (0.5)	0.269 (0.004)	0 (5)	2.1 (1.0)		
Cu/Pd 9:1 foil	Pd	Pd−Cu	[10.8][b]	0.258 (0.002)	0 (4)	2.0 (1.0)	0.4	60
		Pd−Pd	[1.2][b]	0.265 (0.005)	4 (7)	2.5 (1.0)		

[a] Modified FEFF8 backscattering amplitude with Pd foil was used. [b] Square brackets indicate the values obtained from crystallographical data.

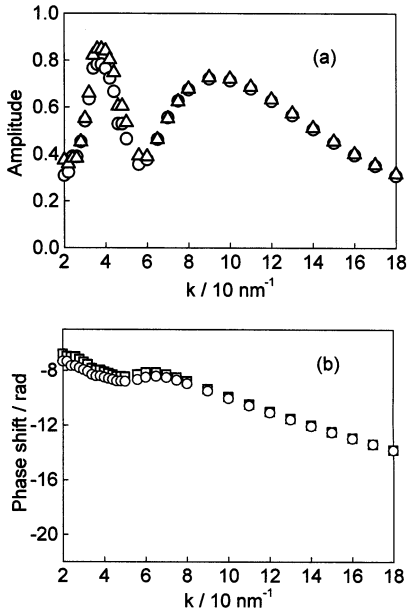

Figure 5. Amplitude (a) and phase shift (b) for a Cu−Pd bond calculated from FEFF8. Open circles and triangles correspond to the amplitudes assuming a Cu lattice (case 1) and a Pd lattice (case 3), respectively. Those for Cu−Pd bond with 11 Cu surroundings in Cu lattice (case 2) are given as open squares.

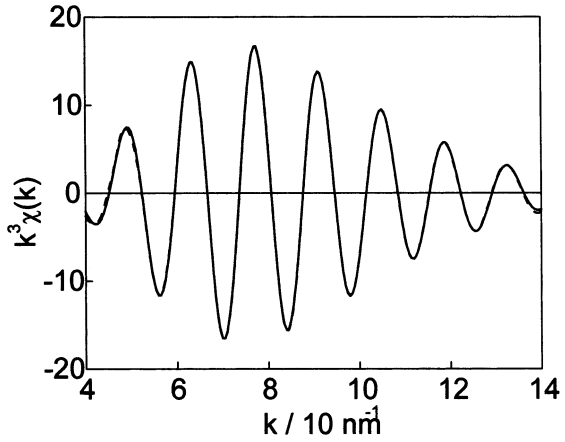

Figure 6. Curve-fitting results of Cu foil using FEFF8-calculated amplitude and phase shift. Solid and broken lines are observed and calculated data, respectively.

there is asymmetric distribution, the r should be further deviated from the peak top by $C_3/(2\sigma^2)$. The σ^2 and C_3 can be calculated from Debye temperature and thermal expansion coefficient for Cu, respectively.[30] Consequently, the deviation amounted to 0.003 nm, well-corresponding to the difference between crystallographic data and EXAFS results. Throughout this paper, we will use eq 1, and hence, EXAFS may give at least 0.003 nm shorter distance than those given by X-ray diffraction.

In the case of Pd fitting, the fitting degree between theoretical and observed spectra was lower than that in the case of Cu. The disagreement between the theoretical and observed spectra was large especially in the low k region below 60 nm^{-1}. Figure 8 shows the backscattering amplitude functions derived from Pd foil and calculated from FEFF8. The empirically derived amplitude function was plotted after the correction of the inelastic reduction factor ($S = 0.7$) and the Debye−Wallor factor. The amplitude derived from FEFF in the range of 30−60 nm^{-1} is quite larger than that determined by Pd foil. Such difference may not be so serious in the analysis of Pd monometallic particles because k^3-weighted $\chi(k)$ could be fitted with a simple sine curve of one Pd−Pd distance mainly in a high k region. However, when we carried out two shell fittings on Cu/Pd bimetallic system, the difference between observed and calculated amplitudes might cause a serious error or large uncertainty in the structure determination because the backscattering amplitude for the Cu−Cu pair has its maximum around 70 nm^{-1}. Thus, we corrected the Cu−Pd backscattering amplitude less than 60 nm^{-1} using empirical values and used the amplitude function for Cu−Pd as shown with an open circle in Figure 8. Figure 7b and Table 1 are the results for Pd foil using this modified Pd−Pd amplitude. The agreements of calculated and observed spectra are much improved, nearly $R = 1.0\%$. Especially, the agreement is improved in a low k region. In the best-fit result, the bond is shorter than crystallographic data by 0.002 nm, which is in good agreement with the value expected from the $2\sigma^2/r^2$ and $C_3/(2\sigma^2)$ corrections.

Next, we carried out the curve-fitting analyses on the Cu/Pd alloy foils using the similarly modified backscattering amplitude for a Cu−Pd bond pair because the backscattering amplitude functions for Pd−Pd and Cu−Pd pairs calculated from FEFF8

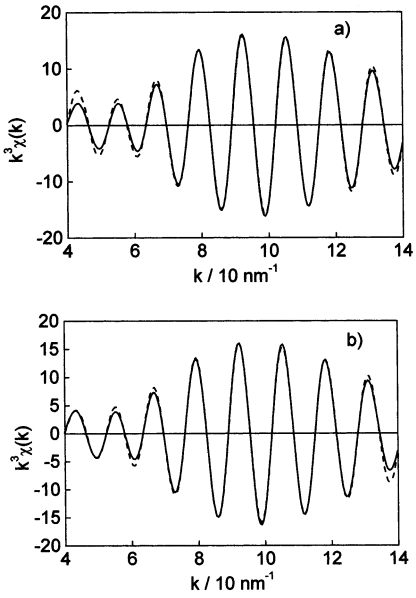

Figure 7. Curve-fitting results of Pd foil using FEFF8-calculated amplitude and phase shift: (a) FEFF8-derived parameters as calculated; (b) modified FEFF8 parameters (see in the text). Solid and broken lines are observed and calculated data, respectively.

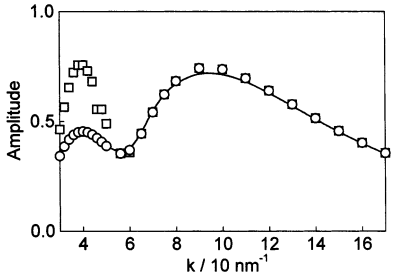

Figure 8. Backscattering amplitude for Pd foil calculated from FEFF8 (open squares) and empirically derived from Pd foil (solid line). Open circles indicate the modified FEFF8 amplitude function using Pd foil.

were not so different from each other (see Figures 5 and 8). Figures 9−11 show the curve fitting results for Cu/Pd alloy foils. In the analysis of Cu K-edge EXAFS of Cu/Pd l:9 foil and Pd K-edge EXAFS of Cu/Pd 9:1 foil, coordination numbers were fixed to the ones expected from the random alloy model with fcc structure (i.e., 1.2 and 10.8 for Cu−Cu and Cu−Pd in Cu/Pd l:9 foil). The error bars for Cu−Cu and Pd−Pd in Cu/Pd 1:9 and 9:1 are a little large, respectively, because of their small contribution. We have determined the *S* factors for all pairs and analyzed the Cu/Pd 1:1 foil, using these *S* factors. The coordination numbers in the Cu−Pd 1:1 foils were almost 6 for all bondings, which agreed with the random alloy model in the Cu/Pd alloy foil. The bond distances for Cu−Pd, Cu−Cu, and Pd−Pd are depicted in Figure 12. The Cu−Cu, Cu−Pd, and Pd−Pd bond distances increase with the Pd composition. The dependence of bond lengths for Cu−Cu, Cu−Pd, and Pd−Pd on the composition can be expressed by the linear lines with their slopes 0.008, 0.013, and 0.008 nm/atom, respectively. The lattice constants for Cu/Pd foil approximately follow Vegard's law.[31] However, the observed Cu−Cu and Pd−Pd distances are much deviated from the expected values of Vegard's law. It is often reported in compound semiconductors and mixed alkaline halides that the change of bond length against composition is smaller than that expected from Vegard's law.[32] However, the lattice constant calculated from the average of bond lengths determined by EXAFS using the following equation are in good agreement

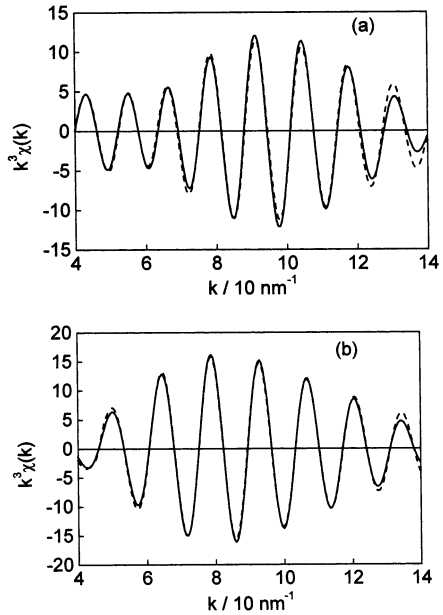

Figure 9. Curve-fitting results of (a) Cu K-edge and (b) Pd K-edge EXAFS for Cu/Pd foil with Cu/Pd = 1:9 using FEFF8-calculated amplitude and phase shift. The Cu−Pd amplitude function in the region lower than 60 nm^{-1} was corrected by the amplitude derived from Pd foil.

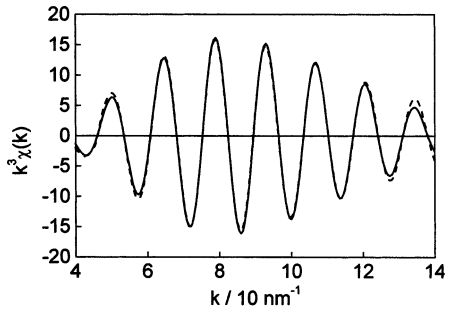

Figure 10. Curve-fitting results of Pd K-edge EXAFS for Cu/Pd foil with Cu/Pd = 9:1.

with those estimated from Vegard's law as shown by filled squares in Figure 12.

$$r(\text{average}) = \sum_{i,j} r_{i-j} N_{i-j} C_i$$

$$i, j = \text{Cu, Pd} \qquad (5)$$

where r_{i-j}, N_{i-j}, and C_i are a bond length and a coordination number for the *j*-th atom around the *i*-th absorbing atom and the atomic fraction of the absorbing atom, *i*, respectively.

3.1.2. EXAFS Results of Monometallic PVP-Stabilized Nanoclusters. Before starting the analysis of the bimetllic nanoclusters, we analyzed the EXAFS oscillations of PVP-stabilized Cu and Pd monometallic nanoclusters. It is often reported that the asymmetric distribution becomes larger when particle sizes decrease.[33,34] Large asymmetric radial distribution causes smaller coordination number and shorter bond distances than real ones. Curve-fitting results are summarized in Table 2. In the case of Cu colloid particle, the coordination number for Cu−Cu was nearly 12, indicating the formation of larger Cu particles, more than 10 nm, which was in good agreement with the previous reports.[6,8] On the other hand, PVP-stabilized Pd nanoclusters gave the coordination numbers to be 8.0 corresponding to the cluster size of nearly 1.5 nm. The bond distance 0.273 nm for Pd−Pd in the Pd nanocluster was almost equal to that of Pd

TABLE 2: Curve-Fitting Results of the PVP-Stabilized Cu and Pd Nanoclusters

sample	edge	bond	N	r, nm	ΔE, eV	$\Delta\sigma^2$, 10^{-5} nm^2	R, %	S/N
Cu colloid	Cu	Cu−Cu	12.5 (0.8)	0.254 (0.002)	4 (5)	4.0 (2.0)	0.7	160
Pd colloid	Pd	Pd−Pd	8.0 (0.6)	0.273 (0.003)	−4 (4)	1.9 (1.5)	0.8	106

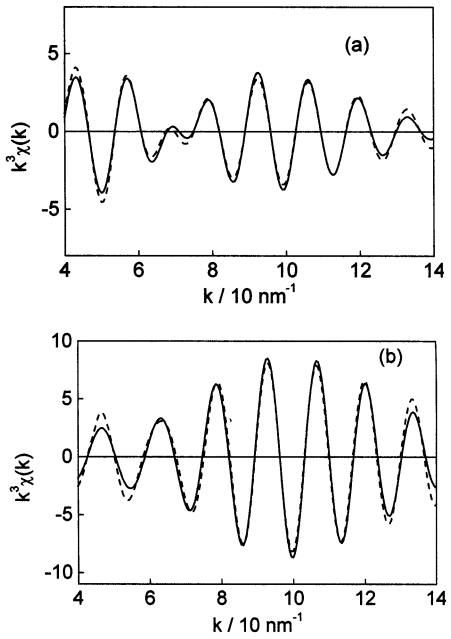

Figure 11. Curve-fitting results of (a) Cu K-edge and (b) Pd K-edge EXAFS for Cu/Pd foil with Cu/Pd = l:l.

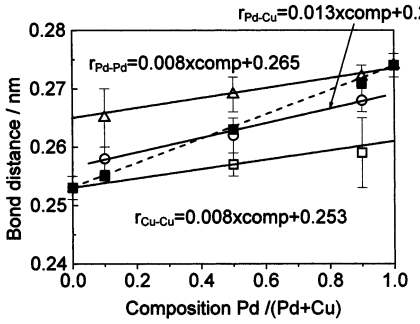

Figure 12. Composition dependence of bond distances in Cu/Pd alloy foils determined by EXAFS. Open squares, open triangles and open circles correspond to Cu−Cu, Pd−Pd, and Cu−Pd bond distances, respectively. Closed squares indicate the average bond distance in the Cu/Pd alloy foil.

foil indicating the contraction due to the formation of fine particles[33−35] seems to be small in the PVP-stabilized 1.5 nm nanocluster. Thus, the effect of asymmetry seems to be smaller than that expected, which will be discussed again in a later stage.

3.1.3. EXAFS Results of Bimetallic PVP-Stabilized Nanoclusters. Figures 13 and 14 show Cu and Pd EXAFS oscillations and the Fourier transforms of k^3-weighted EXAFS for bimetallic cluster samples, respectively. Peak positions of Fourier transforms of Cu K-edge EXAFS oscillations appeared at 0.213 nm for the Cu−Pd 4:1 sample and 0.255 nm for the Cu/Pd 1:4 sample. Compared with Cu and Cu/Pd alloy foil in Figure 3, the Fourier transform peak position indicated the large Cu−Cu contribution in the former sample and a larger Cu−Pd contribution in the latter sample. In the Cu−Pd 3:2 and 1:1 samples, the peak was split due to the interference effect as mentioned above. In the Pd Fourier transform, the main peaks in Cu/Pd 4:1 and 1:4 appeared at 0.22 and 0.246 nm, respectively, indicating the formation of Pd−Cu and Pd−Pd bonds, respectively. These Fourier transforms indicated the formation of Cu/Pd alloy particles in these samples.

TABLE 3: Curve-Fitting Results of the PVP-Stabilized Cu/Pd Bimetallic Nanoclusters

Cu/Pd	edge	bond	N	r, nm	ΔE, eV	$\Delta\sigma^2$, 10^{-5} nm^2	R, %	S/N
4:1	Cu K	Cu−Cu	6.0 (0.5)	0.253 (0.003)	−4 (3)	6.0 (1.0)	1.8	113
		Cu−Pd	1.8 (0.4)	0.258 (0.005)	4 (5)	4.9 (2.0))		
	Pd K	Pd−Cu	7.2 (0.4)	0.257 (0.002)	−2 (3)	2.7 (1.0)	0.4	65
		Pd−Pd	0.8 (0.4)	0.270 (0.005)	6 (4)	1.3 (2.0)		
3.2	Cu K	Cu−Cu	3.9 (0.4)	0.253 (0.004)	−5 (5)	4.5 (2.0)	1.7	190
		Cu−Pd	3.8 (0.4)	0.258 (0.004)	6 (5)	4.6 (2.0)		
	Pd K	Pd−Cu	5.5 (0.5))	0.257 (0.003)	4 (5)	2.4 (2.0)	0.8	63
		Pd−Pd	2.2 (0.5)	0.270 (0.004)	0 (6)	3.7 (2.0)		
1:1	Cu K	Cu−Cu	2.8 (0.5)	0.253 (0.004)	−4 (5)	5.0 (1.0)	2.0	112
		Cu−Pd	5.0 (0.5)	0.258 (0.003)	4 (5)	4.4 (2.0)		
	Pd K	Pd−Cu	5.1 (0.4)	0.259 (0.003)	−2 (5)	2.4 (2.0)	1.3	68
		Pd−Pd	2.8 (0.3)	0.270 (0.003)	7 (6)	2.7 (2.0)		
1:4	Cu K	Cu−Cu	0.8 (0.6)	0.255 (0.005)	−3 (5)	5.5 (3.0)	1.5	27
		Cu−Pd	7.0 (1.0)	0.264 (0.005)	4 (3)	5.0 (3.0)		
	Pd K	Pd−Cu	1.8 (0.4)	0.265 (0.004)	−3 (4)	3.0 (2.0)	1.7	96
		Pd−Pd	6.0 (0.4)	0.273 (0.002)	3 (5)	3.6 (1.0)		

We carried out curve-fitting analyses on these samples. The best-fit results are shown in Figure 15. The fitting results are summarized in Table 3. Table 3 shows that the relationships (eq 4) in the bond length and coordination number between unlike atomic pairs (Cu−Pd and Pd−Cu) are fulfilled within the limit of error for the PVP-stabilized Cu/Pd bimetallic clusters. The Cu−Pd bond distances for Cu/Pd 4:1, 3:2, and 1:1 are shorter than the average value (0.264 nm) of Cu−Cu and Pd−Pd distances, while the Cu−Pd distance in the Cu−Pd 1:4 sample is almost equal to the average value of the two distances. Figure 16 shows the composition dependence of Cu−Cu, Cu−Pd, and Pd−Pd bond distances for bimetallic nanoclusters and foils. Solid lines are least-squares fits for Cu−Cu and Pd−Pd bond distances in Cu/Pd foils and broken lines correspond to those for bimetallic nanoclusters. Smaller slopes in the broken lines indicate that the Cu−Cu and Pd−Pd bond distances in colloid samples are not so different from those found in Cu and Pd foils and nanoparticles. Cu−Pd bond distances in the bimetallic nanoclusters are shorter than those expected from the Cu/Pd foils.

4. Discussion

4.1. Validity of EXAFS Analysis. First of all, we have to discuss the validity of the EXAFS analyses. The origins of systemic errors can be (1) higher harmonics, (2) edge height estimation, (3) background removal, (4) curve-fitting analysis (correlation between fitting parameters), and (5) curve fitting analysis (validity of theoretical parameters). Terms 1−3 are mainly related to the amplitudes and terms 4 and 5 are the origins of errors for the amplitudes and phases.

(1) Higher Harmonics. We had carried out higher harmonics rejection as described in the Experimental Section. Thus, these should be negligibly small.

(2) Edge Height Estimation. We estimated the errors accompanied with edge height estimation to be 0.01 by changing the normalization points. In the Pd K-edge, the edge height was adjusted to be 1. But for the Cu edge, it was difficult to obtain

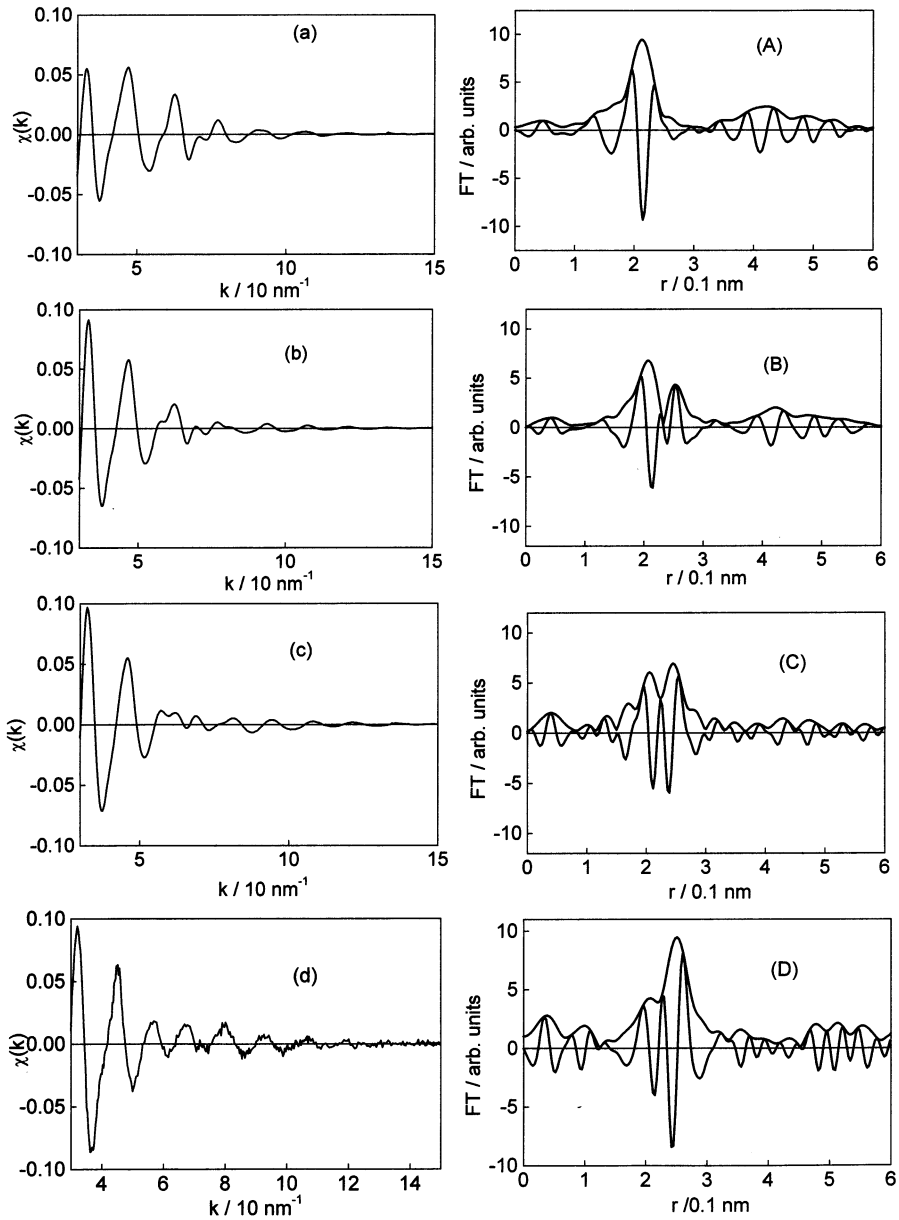

Figure 13. Cu K-edge EXAFS oscillations (a,b,c,d) and the k^3-weighted Fourier transforms (A,B,C,D) of the PVP-stablized Cu/Pd nanoclusters with the composition of (a,A) Cu/Pd = 4:1, (b,B) Cu/Pd = 3:2, (c,C) Cu/Pd = 1:1, and (d,D) Cu/Pd = 1:4.

the edge height to be 1 when we kept the total absorption less than 3. Thus, the edge height for Cu K-edge EXAFS was 0.3 at the lowest for 1:4 Cu/Pd clusters. The error in the coordination number due to the edge height estimation is 3%.

(3) Background Removal Process. Because the spline smoothing method is a strong background removal technique, it often removes an EXAFS signal. We always checked the height of Fourier main peak during the background removal processes. The decrease after the suitable background removal in the main peak was less than 1%.

(4) Correlation Between Fitting Parameters. Error bars accompanied by the fitting procedure were estimated by a χ^2 test according to the international XAFS standards and criteria.[36] The confidence of limit is 65%. The error bars shown in the tables are mainly due to the fitting procedures.

(5) Theoretical Phase and Amplitude Functions. The amplitude of FEFF8 was greater than the empirical values and should be corrected by a *S* factor. We have regarded the *S* factor to be constant and independent of *k*, following the Teo's argument.[37] We determined the *S* factors using EXAFS data of Cu, Pd, and Cu/Pd foils. The values were checked with Cu/Pd 1:1 foils. The determined coordination numbers were in good agreement with those expected for a random alloy model, indicating the validity of the determined *S* factors within the accuracy of less than 5%. Furthermore, we corrected Pd backscattering amplitude using Pd foil data, which improve the fitting result as shown in Figure 7. The other factor that we should consider for the cause of error in amplitude and phase shift is the effect of asymmetric radial distribution. Because of the cut off of the low *k* region, EXAFS gives smaller coordination number and shorter bond distance for a largely disordered system with an asymmetrical radial distribution function.[38] Such a large disorder may be induced by the different bond lengths between the surface and the core of nanocluster, as well as the larger thermal disorder in small particles.[25−27,39] The error in coordination number, sometimes, reached 50% of the total coordination number. However, we thought that the asymmetric distribution was not too large to create the serious errors in the fitting results of this sample for the following reasons. (1) The asymmetric effect would cause the contraction of bond length, but little contraction

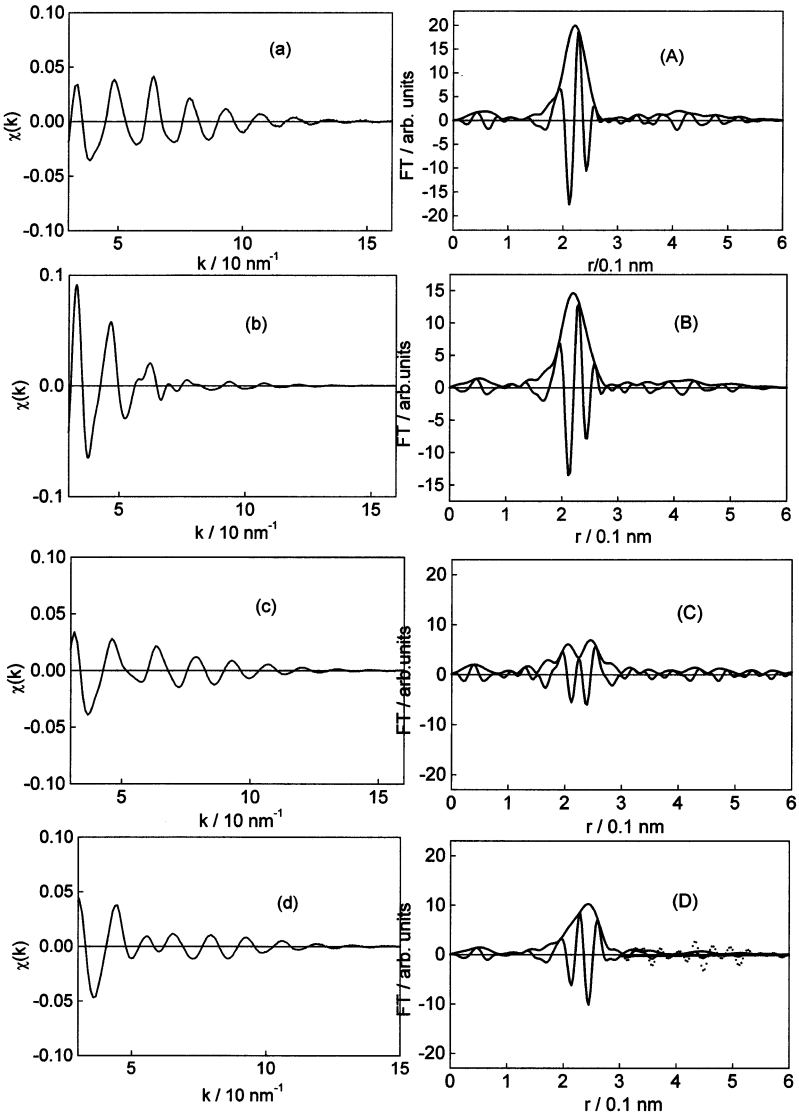

Figure 14. Pd K-edge EXAFS oscillations (a,b,c,d) and the k^3-weighted Fourier transforms (A,B,C,D) of the PVP-stablized Cu/Pd nanoclusters with the compositions of (a,A) Cu/Pd = 4:1, (b,B) Cu/Pd = 3:2, (c,C) Cu/Pd = 1:1, and (d,D) Cu/Pd = 1:4.

of Cu−Cu and Pd−Pd bond distances were observed in the PVP-stabilized monometallic and bimetallic clusters compared to the bond distances in foils. (2) If there were so much disorder, the fitting between observed and calculated should be much worse than those of the foils, but we found the same or a little worse *R*-factors for colloid systems than those in foils. (3) The relation between $r_{Cu-Pd} = r_{Pd-Cu}$ and $N_{Cu-Pd}C_{Cu} = N_{Pd-Cu}C_{Pd}$ should have not been fulfilled in such a largely disordered system.

The less asymmetric distribution effect may be due to the presence of PVP on the cluster surface. It is often reported that the surface reconstruction is lifted when the adsorbates are present on the surface[40,41] and the contraction in the surface bond is recovered to the bulk value by the adsorption of hydrogen.[42] The interaction between PVP and the surface atoms may recover the original bond length. Moreover, the thermal disorder is also reduced because of the presence of the PVP on the surface. Pt particles covered with TiO_x gave smaller thermal disorder than those without TiO_x on the surface.[25] The PVP on the surface of the nanocluster has reduced both static and thermal disorder. The previous successful EXAFS analyses on the PVP-stabilized nanoclusters also owed to the smaller disorder effect in the presence of the surface PVP.[6,14−16,44]

4.2. Comparison with Other Methods. The PVP-stabilized Cu/Pd bimetallic nanoclusters have been examined by HRTEM, XRD, and UV−vis spectra. Cu nanoclusters show a plasmon absorption at 560 nm in the UV−vis spectra, while the Cu−Pd bimetallic sample did not show any absorption band, indicating the formation of alloy particle. XRD patterns also support the bimetallic nanoclusters by monotonic change in the lattice constant from the Cu nanocluster to the Pd nanocluster. In the analysis of EXAFS, the presence of the Pd−Cu bond has clearly shown the formation of Pd−Cu alloy particle. The total coordination number is 7.7 ± 1.0 determined by the present EXAFS analysis. This value is corresponding to a three shell cluster composed of 55 atoms with a diameter of 1.4 nm (the total coordination number of this three shell cluster model is 7.8). This value is quite smaller than the TEM data (5.0 nm).[17,43] The upper limit of the error in the particle-size estimation based on the uncertainty in coordination number is 0.4, corresponding to 1.8 nm particle size. This discrepancy may arise from the following possibilities. (1) the systematic error due to the asymmetric radial distribution function in coordination number determination by EXAFS; (2) the assembly of the bimetallic nanocluster to form a large supercluster.

As discussed in the previous section, the former effect may

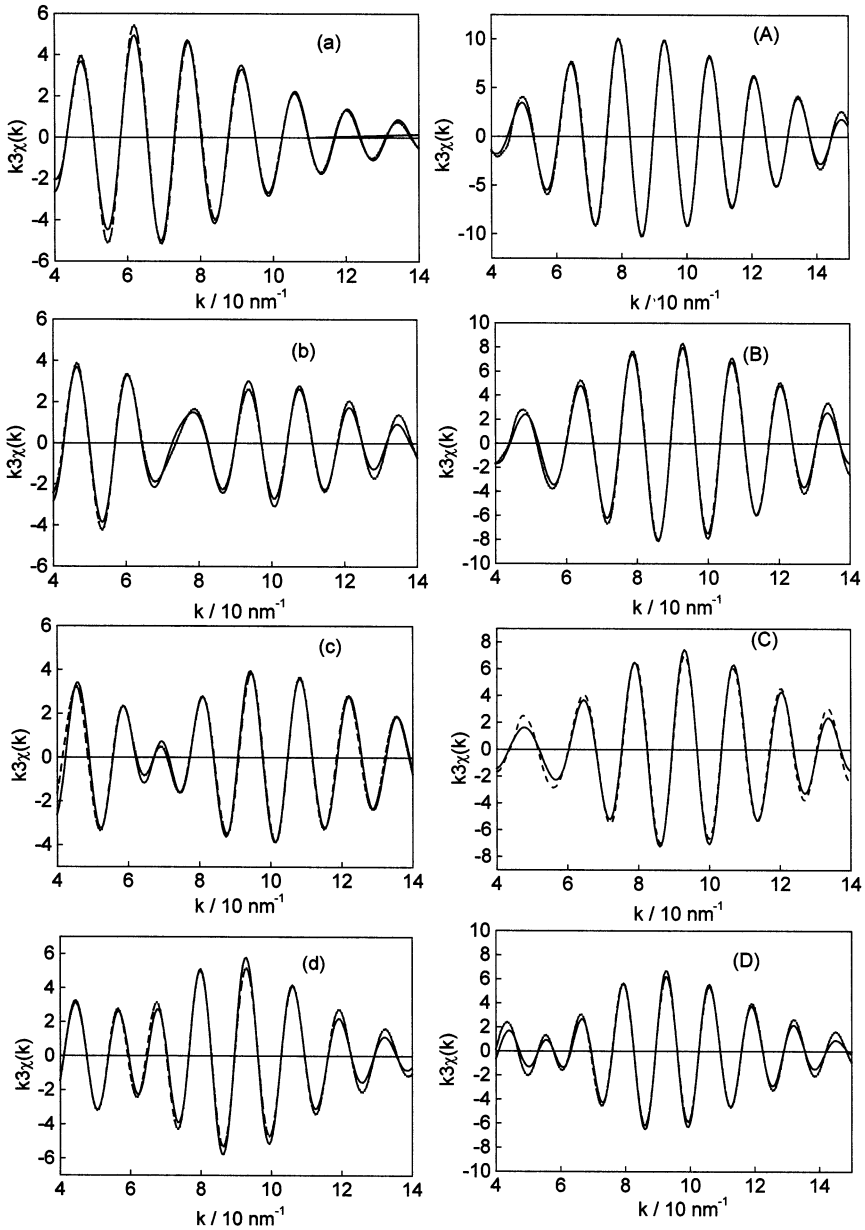

Figure 15. Curve-fitting results of Cu (a,b,c,d) and Pd (A,B,C,D) K-edge EXAFS for the PVP-stabilized Cu/Pd nanoclusters with the compositions of (a,A) Cu/Pd = 4:1, (b,B) Cu/Pd = 3:2, (c,C) Cu/Pd = 1:1, and (d,D) Cu/Pd = 1:4.

not be large in our system. Therefore, we think this discrepancy occurs because of the latter phenomenon, in which Cu/Pd nanoclusters of 1.4 nm (55 atoms) get together to form a larger Cu/Pd assembly. Similar phenomena have been observed in the Rh/Pt system for which EXAFS gave a smaller coordination number than that expected from TEM and small-angle X-ray scattering results.[16,44,45] The RhPt clusters with 55 atoms get together and form a larger assembly with a diameter of 3.0−4.0 nm called a supercluster. Further investigations using TEM and small X-ray angle scattering must be necessary to confirm the formation of the supercluster.

Another discrepancy from the previous observation is the bond length. HRTEM indicated the elongation of the (111) lattice spacing to 0.250 from 0.225 nm in the foil.[17] The proposed possible reason was the large number of surface atoms that were relaxed from their normal crystal lattice positions by the formation of alloy of extra atoms.[17] Lattice spacing of 0.250 nm for (111) corresponds to 0.30 nm for the metal−metal bond distance, which could be observed in the Fourier transform because more than 70% of atoms are located on the surface. But we could not find such an elongated bond distance in the PVP-stabilized Cu/Pd nanoclusters by EXAFS. One possibility to explain the discrepancy is that the observed lattice image with 0.250 nm spacing is corresponding to that of (110), which can give the metal−metal distance at 0.250 nm well-corresponding to those distances in the EXAFS observations. Further investigation must be necessary to understand this phenomenon.

4.3. Structure of CuPd Nanoclusters. Finally, we discuss the inner structure of Cu/Pd bimetallic nanoclusters and relationship with the catalysis. Surface segregation of Cu−Pd alloy foil was observed by XPS and Auger electron spectroscopy (AES).[46] Renourprez et al. reported the location of Cu atoms at surfaces in Cu/Pd nanoparticles on SiO_2 by infrared spectra studies of adsorbed CO.[47] Molenbroek et al. found that Cu enrichment occurred at the surface of Cu/Pd particles on $\gamma-Al_2O_3$ and random alloy was formed on SiO_2 surface.[48] Theoretical calculation also suggests the segregation of Cu to surface.[49] The Pd core and Cu shell model seems to be one possible structure. However, the coordination numbers expected from core−shell models are different from those observed in

TABLE 4: Coordination Numbers Given by EXAFS Analyses and Expected from the Model Structures

					N expected					
							random		heterobond-	
Cu/Pd	edge	bond	*N* obsd	total	core−shell	total	alloy	total	philic	total
4:1	Cu K	Cu−Cu	6.0 (0.5)	7.8 (0.6)	5.0	6.8	6.2	7.8	6.1	7.9
		Cu−Pd	1.8 (0.4)		1.8		1.6		1.8	
	Pd K	Pd−Cu	7.2 (0.4)	8.0 (0.6)	7.3	12	6.2	7.8	7.0	7.7
		Pd−Pd	0.8 (0.4)		4.7		1.6		0.7	
3:2	Cu K	Cu−Cu	3.9 (0.4)	7.7 (0.6)	3.6	6.2	4.7	7.8	3.2	7.4
		Cu−Pd	3.8 (0.4)		2.6		3.1		4.2	
	Pd K	Pd-Cu	5.5 (0.5)	7.7 (0.7)	3.9	10.1	4.7	7.8	6.3	8.5
		Pd−Pd	2.2 (0.5)		6.2		3.1		2.2	
1:1	Cu K	Cu−Cu	2.8 (0.5)	7.8 (0.7)	3.1	6.1	3.9	7.8	2.7	7.8
		Cu−Pd	5.0 (0.5)		3.0		3.9		5.1	7.8
	PdK	Pd−Cu	5.1 (0.4)	7.9 (0.5)	2.9	9.5	3.9	7.8	5.1	7.8
		Pd−Pd	2.8 (0.3)		6.6		3.9		2.7	7.8
1:4	CuK	Cu−Cu	0.8 (0.6)	7.8 (1.0)	0.9	5.3	1.6	7.8	0.7	7.7
		Cu−Pd	7.0 (1.0)		4.5		6.2		7.0	
	Pd K	Pd−Cu	1.8 (0.4)	7.8 (0.6)	7.4	8.5	1.6	7.8	1.8	7.9
		Pd−Pd	6.0 (0.4)		1.1		6.2		6.1	

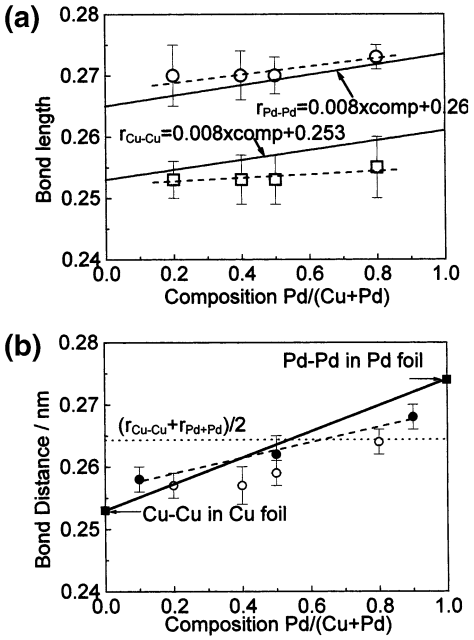

Figure 16. Composition dependence of the (a) Cu−Cu and Pd−Pd and (b) Cu−Pd bond distances in the PVP-stabilized Cu/Pd bimetallic nanoclusters determined by EXAFS. Solid lines in panel a are least-squares fitted lines of Cu−Cu and Pd−Pd bond distances in Cu/Pd alloy foils as shown in Figure 12. Broken lines in panel (a) are those in the bimetallic nanoclusters. Open circles in panel (b) correspond to Cu−Pd bond distances in the bimetallic nanoclusters. Dotted line indicates the average value of Cu−Cu and Pd−Pd bond distances (0.264 nm). Cu−Cu and Pd−Pd bond distances in Cu and Pd foils are shown in filled squares and connected by a solid line, which corresponds to the Vegard's law. Broken line is a least-squares fit of the Cu−Pd bond distances (small dots) in Cu/Pd alloy foils determined by EXAFS.

the EXAFS analyses, as shown in Table 4. Thus, in the case of Cu/Pd nanocluster, the core−shell model is inappropriate as a model structure. Other typical structures proposed hitherto are alloy and cluster-in-cluster models. In the latter model structure, the coordination numbers for like atoms such as Cu−Cu and Pd−Pd (homobond pair) should be larger than those for unlike atoms such as Cu−Pd and Pd−Cu (heterobond pair). Thus, this cluster-in-cluster structure can be said to be a "homobond-philic" structure. But the observation is reverse. The alloy model gives the coordination numbers being well proportional to those of compositions. Bradley et al. carried out EXAFS analyses on

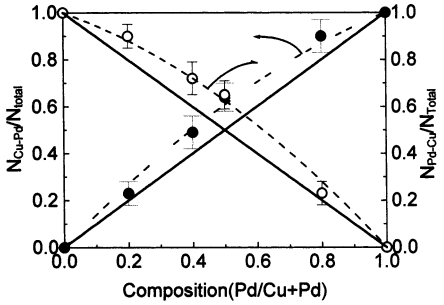

Figure 17. Composition dependence of Cu−Pd (filled circles) and Pd−Cu (open circles) coordination numbers together with that expected from a random alloy model (solid line). Broken lines are the least-squares fit of the data.

5.0 nm PVP-protected colloidal Pd/Cu alloys with the composition $Cu_{0.1}Pd_{0.9}$ and $Cu_{0.2}Pd_{0.8}$ prepared by a direct reduction of Cu(II) and Pd(II) and a plating method of Cu(II) on the presynthesized Pd colloidal particles.[50] They found that Cu(II) was completely reduced to zero-valent and existed in the core region of Pd/Cu alloy to form Cu−Pd bonds even in the plating method, indicating the good miscibility of the two elements. Figure 17 shows the relation between coordination numbers and compositions of bimetallic nanoparticles. The observed ratio of the Cu coordination number around Pd or that of Pd around Cu (i.e., homobond) to the total coordination numbers ($N_{Cu-Pd} + N_{Cu-Cu}$) were always larger than the linear line with a slope of 1 that was expected from the random alloy model. Moreover, Cu−Pd bond distances found in 4:1, 3:2, and 1:1 Cu/Pd bimetallic nanoclusters were shorter than those expected, as shown in Figure 16. These facts indicate the preferential formation of the unlike atom pair. Cu and Pd are known to form intermetallic compounds such as Cu_3Pd and CuPd in which more Cu−Pd bonds are present than Cu−Cu and Pd−Pd bonds.[31] Such an intrinsic factor causes the preferential Cu−Pd bond formation in Cu−Pd nanoparticles. We now propose a "heterobond-philic" structure model for Cu/Pd bimetallic nanocluster rather than the simple random alloy model. To demonstrate that the coordination numbers observed in XAFS analyses are realistic, we have conducted a very simple Monte Carlo calculation to construct a Cu/Pd bimetallic model structure in the following hypotheses. (1) A lattice structure for Cu/Pd nanocluster is fcc. (2) A nanocluster with 55 atoms is postulated with the appropriate Cu/Pd ratio (1:4, 1:1, 3:2, 4:1). (3) Each atom is fixed at a lattice point. (4) Bond energies of Cu−Cu

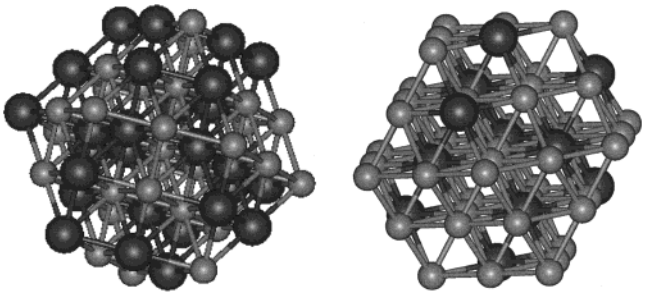

Figure 18. Model structures for Cu/Pd l:l (left panel) and Cu/Pd 4:1 (right panel) nanoclusters. Big dark balls correspond to Pd.

and Pd−Pd are smaller than that of Cu−Pd. (5) The total energy is calculated only by summing the first neighbor bond energies. (6) Cu and Pd positions are randomly replaced, and the minimum of total energy is surveyed using a Metropolis method.

The hypothesis 4 is rationalized by the fact that the formation enthalpy of CuPd solution at 1350 K is negative, about −11 kJ/mol.[31] We used the bond energies $E/RT = 0$ for Cu−Cu and Pd−Pd and $E/RT = 4 \sim$ (10 kJ/mol) for Cu−Pd in the calculation.

After getting the equilibrium structure with a certain total energy, we pick up a structure as a typical model which is shown in Figure 18. We also calculated the coordination numbers, which are listed in Table 4. The larger coordination numbers for heterobonds than those for homohonds are reproduced in the model structure. Moreover, the absolute values of the calculated coordination numbers fit the observed ones farely well. Even if calculation is very rough, we can say that the coordination numbers derived from EXAFS are realistic and strong Cu−Pd bonds cause the heterobond-philic nanocluster structure.

The PVP-stabilized Cu/Pd nanoclusters catalyzed CH_2═CH−CN hydration to form CH_2═CH−$CONH_2$, selectively.[11] The formation rate increased with the increase of Cu/Pd ratio between 1 and 3. The 4:1 Cu/Pd nanoclusters showed a higher reaction rate per Cu atom than that of 1:1 Cu/Pd nanoclusters, while hydrogenation reaction of 1,3-cyclooctadiene has no activity on that 4:1 Cu/Pd cluster. Surface Cu−Pd ensembles were speculatively proposed for the active site for the hydration reaction, where CH_2═CH−CN adsorbed on a Pd site was effectively attacked by water adsorbed on a Cu site.[8] As shown in Figure 18, surface Pd is more surrounded by surface Cu atoms in a 4:1 Cu/Pd nanocluster (right panel), while surface Pd−Pd ensembles are still present in a 1:1 Cu/Pd nanocluster (left panel). At the same time, the 4:1 Cu/Pd nanocluster did not show the hydrogenation reaction probably because the Pd−Pd ensemble must be necessary for supplying both hydrogen and hydrocarbon adsorption sites. Therefore, the preferential tendency to form Cu−Pd bonds effectively creates the Cu/Pd ensemble, which may be the active site for the selective hydration reaction.

5. Conclusions

PVP-stabilized Cu/Pd nanoclusters prepared through Cu/Pd hydroxides have a "heterobond-philic" alloy structure with Cu−Pd bonds being preferentially formed. Cu−Cu, Pd−Pd, and Cu−Pd distances are dependent on the Cu/Pd composition and the Cu−Pd bond distance is a little shorter than those expected, indicating the stronger interaction between Cu and Pd. The total coordination number indicated that the size of nanoclusters are about 1.2−1.4 nm.

Acknowledgment. The EXAFS measurements were performed under the approval of PAC (Program Advisory Committee, Proposal No. 95G003). We thank Prof. M. Nomura and Dr. T. Usami in Photon Factory for their technical help. One of the authors (L.B.) was financially supported from JICA (Japan International Cooperation Agency) in its program for the training course of developing country. The work was also financially supported by CREST (Core Research Evolution in Science and Technology) of JST (Japanese Corporation of Science and Technology).

References and Notes

(1) Kubo, R. *J. Phys. Soc. Jpn.* **1962**, *17*, 975.
(2) *Ultra-Fine Particles*: *Exploratory Science and Technology*; Hayashi, C., Uyeda, R., Tasaki, A., Eds.; Noyes Publications: Westwood, NJ, 1996.
(3) Schmid, G. *Chem. Rev.* **1992**, *92*, 1709.
(4) Toshima, N. *Macromol. Symp.* **2000**, *156*, 45.
(5) Toshima, N. *Supramol. Sci.* **1998**, *5*, 395.
(6) Toshima, N.; Yonezawa, T. *New J. Chem.* **1998**, *22*, 1179.
(7) Toshima, N.; Wang, Y. *Chem. Lett.* **1993**, 1611.
(8) Toshima, N.; Wang, Y. *Adv. Mater.* **1994**, *6*, 245.
(9) Bradley, J. S.; Hill, E. W.; Klein, C.; Chaudret, B.; Duteil, A. *Chem. Mater.* **1993**, *5*, 254.
(10) Esumi, K.; Tano, T.; Torigoe, K.; Meguro, K. *Chem. Mater.* **1990**, *2*, 564.
(11) Toshima, N.; Wang, Y. *Langmuir* **1994**, *10*, 4574.
(12) Sayers, D. E.; Stern, E. A.; Lytle, F. *W. Phys. Rev. Lett.* **1971**, *27*, 1204. *X-ray absorption, Principles, applications, techniques of EXAFS, SEXAFS, and XANES*, Koningsberger, D. C., Prins, R., Eds.; John Wiley & Sons: New York, 1988; Vol. 92. *X-ray absorption fine Structure for catalysts and surfaces*; Iwasawa, Y., Ed.; World Scientific: Singapore, 1996; Vol. 2, p 410.
(13) Via, G. H.; Drake, K. F.; Meitzner, G.; Lytle, F. W.; Sinfelt, J. H. *Catal. Lett.* **1990**, *5*, 25.
(14) Toshima, N.; Harada, M.; Yonezawa, T.; Kushihashi, K.; Asakura, K. *J. Phys. Chem.* **1991**, *95*, 7448.
(15) Toshima, N.; Harada, M.; Yamazaki, Y.; Asakura, K. *J. Phys. Chem.* **1992**, *96*, 9927.
(16) Harada, M.; Asakura, K.; Ueki, Y.; Toshima, N. *J. Phys. Chem.* **1993**, *97*, 10742.
(17) Lu, P.; Dong, J.; Toshima, N. *Langmir* **1999**, *15*, 7980.
(18) Asakura, K.; Yamazaki, Y.; Kuroda, H.; Harada, M.; Toshima, N. *Jpn. J. Appl. Phys.* **1993**, *32-2*, 448.
(19) Nomura, M.; Koyama, A. *KEK Rep.* **1996**, *95-15*.
(20) Nomura, M.; Koyama, A. *KEK Rep.* **1989**, *89-16*.
(21) Asakura, K. In *X-ray Absorption Fine Structure for Catalysts and Surfaces*; Iwasawa, Y., Ed.; World Scientific: Singapore, 1996; Vol. 2, p 33.
(22) Rehr, J. J.; Albers, R. C. *Rev. Mod. Phys.* **2001**, *72*, 621.
(23) Newville, M.; Boyanov, B. I.; Sayers, D. E. *J. Synchrotron Radiat.* **1999**, *6*, 264.
(24) Bunker, G. *Nucl. Instrum. Methods* **1983**, *207*, 437.
(25) Yokoyama, T.; Asakura, K.; Iwasawa, Y.; Kuroda, H. *J. Phys. Chem.* **1989**, *93*, 8323.
(26) Hansen, L. B.; Stoltze, P.; Borskov, J. K.; Clausen, B. S.; Niemann, W. *Phys. Rev. B* **1990**, *64*, 3155.
(27) Clausen, B. S.; Crabaek, L.; Topsoe, H.; Hansen, L.; Stoltze, P.; Norskov, J. K.; Nielsen, O. H. *J. Catal.* **1993**, *141*, 368.
(28) Teo, B. K.; Lee, P. A. *J. Am. Chem. Soc.* **1979**, *101*, 2815.
(29) Rehr, J. J.; Mustre de Leon, J.; Zabinsky, S. I.; Albers, R. C. *J. Am. Chem. Soc.* **1991**, *113*, 5135.
(30) Yokoyama, T. In *X-ray Absorption Fine Structure for Catalysts and Surfaces*; Iwasawa, Y., Ed.; World Scientific: Singapore, 1996; Vol. 2, p 33.
(31) Predel, B. In *Landolt Boernstein New Series*; Madelung, O., Ed.; Springer Verlag: Berlin, 1994; Vol. IV-5d, p 217.
(32) Mikkelsen, J. C., Jr.; Boyce, J. B. *Phys. Rev. B* **1983**, *28*, 7130.
(33) Yokoyama, T.; Kimoto, S.; Ohta, T. *Jpn. J. Appl. Phys.* **1989**, *28*, L851.
(34) Kuroda, H.; Yokoyama, T.; Asakura, K.; Iwasawa, Y. *Faraday Discuss.* **1991**, *92*, 189.
(35) Apai, G.; Hamilton, J. F.; Stohr, J.; Thompson, A. *Phys. Rev. Lett.* **1979**, *43*, 165.
(36) IXS Report on the International Workshops on Standards and Criteria in XAFS. In *Proceedings of the 6th International Conference on X-ray Absortion Fine Structure*; Hasnain, S., Ed.; Ellis Horwood: New York, 1991; p 751.
(37) Teo, B. K. *EXAFS*: *Basic principles and data analysis*; Springer-Verlag: Berlin, 1986.

(38) Crozier, E. D.; Rehr, J. J.; Ingalls, R. In *X-ray absorption, Principles, applications, techniques of EXAFS, SEXAFS, and XANES*; Koningsberger, D. C., Prins, R., Eds.; John Wiley & Sons: New York, 1988; Vol. 92, p 373.

(39) Sandstrom, D. R.; Marques, E. C.; Biebesheimer, V. A.; Lytle, F. W.; Greegor, R. B. *Phys. Rev. B* **1985**, *32*, 3541.

(40) Gardner, P.; Tueshaus, M.; Martin, R.; Bradshaw, A. M. *Surf. Sci.* **1990**, *240*, 112.

(41) Behm, R. J.; Thiel, P. A.; Norton, P. R.; Ertl, G. *J. Chem. Soc.* **1983**, *78*, 7437.

(42) Moraweck, B.; Clugnet, G.; Benouprez, A. J. *Surf. Sci.* **1979**, *81*, L631.

(43) Note that other old TEM data presented in ref 7 agree with the EXAFS results presented here.

(44) Harada, M.; Asakura, K.; Toshima, N. *J. Phys. Chem.* **1994**, *98*, 2653.

(45) Hashimoto, T.; Saijyo, K.; Harada, M.; Toshima, N. *J. Chem. Phys.* **1998**, *109*, 5627.

(46) Kumar, T. S. S.; Hedge, M. S. *Appl. Surf. Sci.* **1985**, *20*, 290.

(47) Renouprez, A.; Lebas, K.; Bergeret, G. *J. Mol. Catal. A: Chem.* **1997**, *120*, 217.

(48) Molenbroek, A. M.; Haukka, S.; Clausen, B. S. *J. Phys. Chem. B* **1998**, *102*, 10680.

(49) Mukherjee, S.; Moran-Lopez, J. L. *Surf. Sci.* **1987**, *189*/*190*, 1135. Mukherjee, S.; Moran-Lopez, J. L. *Surf. Sci. Lett.* **1987**, *188*, L742.

(50) Bradley, J. S.; Via, G. H.; Bonneviot, L.; Hill, E. W. *Chem. Mater.* **1996**, *8*, 18953.